Transp Porous Med (2016) 112:21–37
DOI 10.1007/s11242-016-0623-0

A New Model for Determining the Effective Permeability of Tight Formation

Renyi Cao[1] · Yang Wang[1] · Linsong Cheng[1] · Y. Zee Ma[2] · Xiaofeng Tian[1] · Na An[1]

Received: 7 April 2015 / Accepted: 5 January 2016 / Published online: 4 February 2016

Abstract Unlike conventional reservoirs, tight reservoirs have complex pore structures and severe boundary-layer effect. The pore throat of tight reservoirs is in nanoscale and the boundary layer cannot be ignored because the boundary layer has an important effect to the fluid flow and its influence increases with the reduction in the pore throat radius. These are the main reasons for the ultra-low permeability and low oil recovery for these reservoirs. However, previous studies have paid limited attention to the influences of the boundary-layer effect and the pore size distribution. In this paper, a new model was built to determine the effective permeability for the tight gas and oil reservoirs by taking into account the boundary-layer effect and the pore distribution. The results from this new model show good agreement with the experiment data, and the main factors that impact the effective permeability were analyzed in the study. It is found that the fluid type, means and standard deviation of pore radius, and displacement pressure gradient are the main factors influencing effective permeability. The relationship of air permeability and liquid permeability is also analyzed for tight reservoirs.

Keywords Tight formation · Effective permeability · Pore size distribution · Boundary layer · Gas slippage

List of symbols

r	Pore throat radius (μm)
ν	Mean pore radius (μm)
σ	Standard deviation (μm)
$f(r_i)$	The proportion of micro-tubes of radius r_i (%)
N	The total number of the micro-tubes

✉ Renyi Cao
caorenyi@126.com

[1] School of Petroleum Engineering, China University of Petroleum, Beijing 102249, China

[2] Schlumberger, Denver, CO 80202, USA

A	The cross-sectional area of the rock (μm^2)
μ	Oil viscosity (mPa s)
τ	Pore structure coefficient
ΔP	Pressure difference (MPa)
ϕ_m	Porosity (%)
p_o	Barometric pressure (MPa)
μ/ε	Slip coefficient ($1/\mu m$)

1 Introduction

Considerable efforts have been made on the recovery of the tight oil as part of developing unconventional resources in the last decade or so, and oil from tight reservoirs represent an increasing share of the world's hydrocarbon source. Tight oil reservoirs have ultra-low permeability, which presents greater challenges for field development in general and for oil recovery in particular. The main reasons for low permeability of tight oil reservoirs include the complex distribution of the pore structures and boundary-layer effect in the pore throats of these reservoirs. In tight oil reservoirs, most pore throats are highly rugose. As the rugosity inevitably increases the length of the path for fluid flow, the resistance would be extremely high for the fluid flow. Moreover, the boundary-layer effect is a problem. The interaction between the solid particles and the liquid is very strong so that a layer of liquid will be attached on the inner surface of the pore and restricts the flow.

For conventional reservoirs, pore throats are relatively uniform, and in fact, uniform pore radius is often used to describe the distribution of pore throats. A number of permeability models have been proposed.

Kozeny (1927) and Carman (1937) built the equivalent capillary model for matrix, which is a simplified representation of the rock and plays a fundamental role in characterizing reservoir permeability. Purcell (1949) derived an equation showing the relationship of permeability to capillary pressure curve. Burdine (1953) calculated the relative permeability from pore size distribution data and used the tortuosity factor in the permeability equation as a term of correction for the difference between the theoretical model and the actual rock. Brooks and Corey (1966) modified the representation of capillary pressure function to a more general form and obtained a new formation of permeability function because of the limitation of Corey's model (1954). However, for tight oil reservoirs, the pore throat distribution is distinct from the conventional reservoirs and displays the feature of heterogeneity. Many experiments have shown that the pore distribution of the tight oil reservoirs exhibits a wide range (Youssef et al. 2007; Riepe et al. 2011; Li et al. 2012; Wang et al. 2009; Nelson 2009; Desbois et al. 2011; Camp 2011). Thus, high deviations may occur when calculating the permeability of tight oil reservoirs while assuming a uniform distribution (Bernabé and Bruderer 1998; Latour et al. 1995; Banavar and Johnson 1987) and the micro-tube model based on uniform radius is not suitable to the determination of permeability for tight reservoirs.

There are still rare reports about the inclusion of pore size heterogeneity in permeability model. It is possible to use a function to represent the distribution, and such a function has the potential advantage of integrating all the variables related to the pore throat and permeability.

Another factor influencing the permeability of the tight reservoirs is the boundary-layer effect, and the boundary layer will reduce the effective flowing space of the micro-tubes and constrain fluid flow. The conception of boundary-layer effect for flow in porous media was first proposed by Мархасин И Л (1977). He supposed there was a thin layer of liquid

on inner surface of the pore because of the interaction of the solid and the liquid. Li et al. (2011) and Mala and Li (1999) conducted micro-tube experiment with deionized water, which proved the existence of boundary layer. Some previous experiment results (Li and He 2005; Zhang et al. 2008; Xu and Yue 2007) showed that the proportion of the boundary layer was controlled by several factors, such as radius of the micro-tube and liquid viscosity.

For tight reservoirs, the scale of the pore throat is mainly in microscale and nanoscale so that the effect of boundary layer on fluid flow in tight reservoirs is obvious. The comparison between gas permeability and liquid permeability is a good case for the impact of boundary layer on permeability measurement of the same reservoir. There exists gas slippage effect (Sampath and Keighin 1982; Daixun 2002; Carman 1956) when gas transports in the pore throats so that the boundary-layer effect is negligible. Gas permeability is normally larger than liquid permeability (Klinkenberg 1941; Dabbous et al. 1974; Li and Horne 2001, 2004). In general, people use gas permeability to represent the permeability of tight reservoirs for its convenience to obtain. However, this is usually not recommended for its inaccuracy. Boundary-layer effect has been ignoring in the permeability expression, which may develop deviation in application especially for tight reservoirs.

The objective of this paper is to propose a new method for calculating the effective permeability of tight formation considering the pore distribution, which plays crucial roles for the tight formation. And also, the boundary-layer effect, which is obvious in nano- or micropores, is included in the calculation of the effective permeability. This paper aims to introduce a conception that pore distribution and boundary-layer effect, which are rarely considered in the previous work, are really essential to permeability of tight formation and cannot be neglected. We use the experimental results to verify the accuracy of this model and discuss the influential variables based on factor analysis with the new model. The results show this model has enough accuracy and can be used in practice for its convenience and simplicity.

2 Modeling

For the convenience of model description, the following assumptions are made for the modeling:

1. The model consists of a bunch of micro-tubes in serial radii and there is sealed volume between micro-tubes;
2. Fluid and rock are incompressible;
3. The flow in reservoirs conforms to Darcy's law and the flow in the micro-tubes satisfies Poiseuille Equation;
4. The throat size distribution can be represented by a function, such as Gaussian distribution;
5. The pore throat distribution is based on the mercury experiment and can be used to represent the heterogeneity of the rock.

2.1 Boundary Layer Effect on Effective Pore Radius and Permeability

Tight oil reservoirs contain a large ratio of pores to throats, and the nanothroat is one of the main constraints for fluid flow in the reservoirs. Figure 1 illustrates the nanothroats in tight oil reservoirs. The effective flow radius for the nanoscale throats may be in the magnitude of only several liquid molecules (such as in heavy oil).

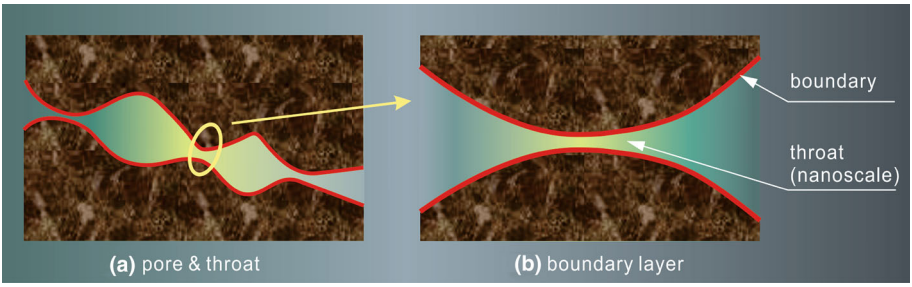

Fig. 1 Schematic of nanoscale pore throats in tight oil reservoirs

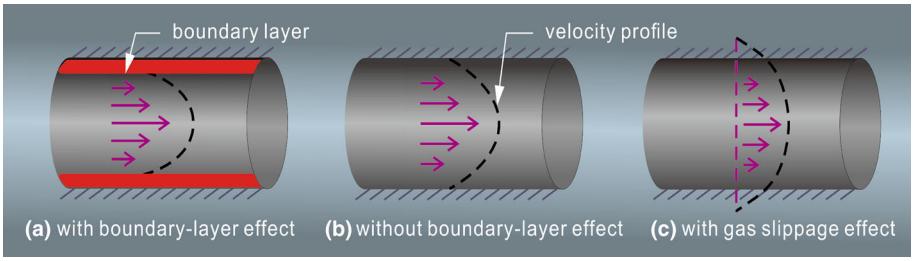

Fig. 2 Schematic of fluid flow profile in porous media

Due to the strong interaction between liquid and solid particles, there will be a thin layer of liquid attached to the pore throat surface. It is really difficult for the boundary layer liquid to flow. Although the thickness of boundary layer is nanoscale for tight oil reservoirs, it may be equivalent to the nanothroat radius. Figure 2 compares the fluid flows with boundary layer and without boundary layer. For the same pore throat space, the effective flow space is quite different between the two models. The flow space will be much narrower for the condition with the boundary layer. Thus, its existence will inevitably constrain the fluid flow, and in some situations even make the flow impossible.

Experimental data (Yang et al. 2012) have indicated that there is no linear relationship between gas permeability and liquid permeability. This is because the boundary-layer effect can be neglected and gas slippage effect dominates during gas flow, so that all pore throats can be regarded as contributing to the permeability; while for the liquid flow, only the PTR much larger than the thickness of the boundary layer can significantly contribute to permeability. The effective pore throat for flow can be obtained by considering the thickness of the boundary layer from the actual pore throat. Figure 3 shows the ratio of gas permeability and liquid permeability, and as seen, it is very large when the gas permeability is low. This ratio will decrease rapidly with the increase in the gas permeability and becomes a constant for high permeability. This phenomenon suggests that the boundary layer will have a significant effect in the low-permeability reservoirs, especially the tight oil reservoirs. Its influence can be neglected in high-permeability reservoirs.

2.2 Expression of Boundary Layer from Micro-tube Experiments

2.2.1 Experimental Setup

Li et al. (2011) conducted the micro-tube experiments with the setup as shown in Fig. 4. It consists of pressure supply unit, measurement unit, pressure system and temperature system.

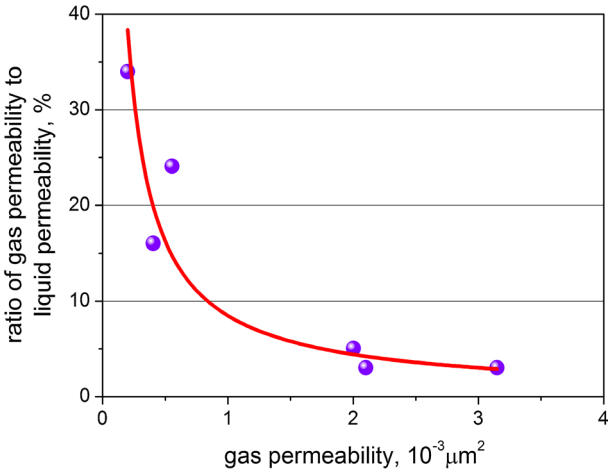

Fig. 3 Relationship between the ratio of gas permeability to liquid permeability and gas permeability

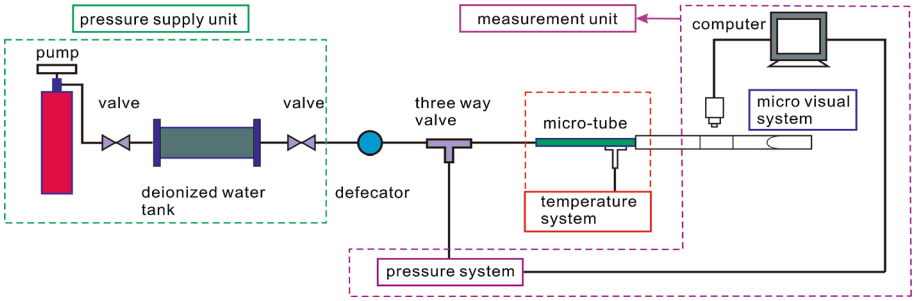

Fig. 4 Micro-tube experimental setup (Redraw from Li et al. 2011)

The deionized water used in the experiment needs to be defecated with the defecator before it goes through the micro-tube. The whole process is conducted at the room temperature. The micro visual system is used to measure the flow rate accurately.

2.2.2 Representation of the Thickness of Boundary Layer

We analyzed a large amount of micro-tube experiment data within micrometer scale and results of Dissipative Particle Dynamics simulation within nanometer scale (Li et al. 2011; Tian et al. 2014). Table 1 lists the parameters and results of the micro-tube experiments (Li et al. 2011). The micro-tube experiment shows that the thickness of the boundary layer is in an exponential relationship with the micro-tube radius and the displacement pressure gradient, and it is in linear relationship with the liquid viscosity. However, when the displacement pressure gradient is greater than 1 MPa/m, the ratio between the thickness of the boundary layer and the micro-tube radius is almost constant. The empirical equation of the thickness of the boundary layer can be expressed as a function of the micro-tube radius and the displacement pressure gradient:

$$h_i = \begin{cases} r_i \cdot 0.25763\mathrm{e}^{-0.261 r_i} (\nabla P)^{-0.419} \cdot \mu, & \nabla P < 1\,\mathrm{MPa/m} \\ r_i \cdot 0.25763\mathrm{e}^{-0.261 r_i} \cdot \mu, & \nabla P > 1\,\mathrm{MPa/m} \end{cases} \quad (1)$$

Table 1 Results and parameters of the micro-tube experiment (Data digitized from Li et al. 2011)

Case1		Case2		Case3		Case4		Case5	
$r = 2.5\,\mu m$ ∇P (MPa/m)	$\mu = 1\,mPa\,s$ v (mm/s)	$r = 5.0\,\mu m$ ∇P (MPa/m)	$\mu = 1\,mPa\,s$ v (mm/s)	$r = 7.5\,\mu m$ ∇P (MPa/m)	$\mu = 1\,mPa\,s$ v (mm/s)	$r = 10\,\mu m$ ∇P (MPa/m)	$\mu = 1\,mPa\,s$ v (mm/s)	$r = 5.0\,\mu m$ ∇P (MPa/m)	$\mu = 1.5\,mPa\,s$ v (mm/s)
0.01	0.001	0.013	0.023	0.011	0.069	0.011	0.127	0.015	0.015
0.03	0.005	0.026	0.034	0.022	0.103	0.022	0.231	0.029	0.022
0.05	0.011	0.04	0.056	0.034	0.149	0.033	0.335	0.044	0.037
0.08	0.02	0.053	0.079	0.045	0.195	0.044	0.462	0.058	0.052
0.099	0.038	0.067	0.113	0.055	0.253	0.055	0.601	0.073	0.075
0.149	0.072	0.08	0.148	0.066	0.322	0.067	0.728	0.088	0.097
0.199	0.115	0.094	0.159	0.077	0.391	0.078	0.866	0.103	0.104
0.241	0.145	0.106	0.205	0.098	0.576	0.09	1.005	0.117	0.135
0.28	0.186	0.121	0.25	0.11	0.656	0.101	1.155	0.133	0.165
0.635	0.855	0.146	0.319	0.121	0.772	0.123	1.444	0.161	0.21
1.252	1.282	0.174	0.387	0.142	0.922	0.146	1.733	0.191	0.255
1.851	1.709	0.2	0.467	0.153	1.002	0.168	2.022	0.22	0.308
2.45	1.709	0.214	0.513	0.165	1.095	0.179	2.195	0.236	0.338
3.049	2.137	0.241	0.64	0.198	1.36	0.202	2.507	0.265	0.421
3.784	2.564	0.268	0.72	0.208	1.452	0.225	2.831	0.294	0.474
4.356	2.991	0.389	3.487	0.544	3.205	0.266	3.846	0.718	2.294
4.927	3.856	1.443	7.051	0.98	5.769	0.381	7.051	1.312	4.639
		1.824	8.333	1.497	8.974	0.653	10.256	1.658	5.482
		2.532	11.539	2.015	11.539	0.98	14.103	2.302	7.591
		2.995	13.462	3.022	17.308	1.388	20.513	2.722	8.856
		3.457	16.026	3.92	23.077	1.661	23.718	3.143	10.543
		4.165	17.949	4.546	26.282	2.559	35.256	3.787	11.808
		4.927	21.154	4.927	28.846	3.838	54.487	4.479	13.917
		5.771	25.082	5.635	32.692	5.172	72.436	5.247	16.447

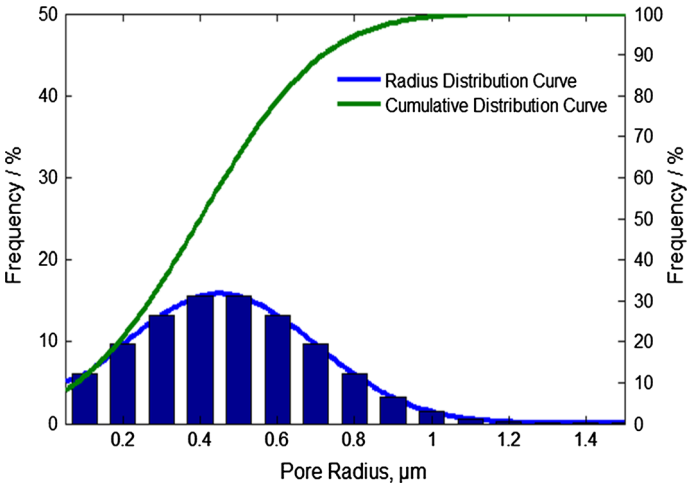

Fig. 5 Pore distribution model in tight reservoirs

It should be noted that the thickness of boundary layer is related to fluid property and rock interfacial property, and thus, h_i in Eq. 1 should be determined based on the experimental results or DPD simulation. The expression of boundary layer thickness belongs to the curve fitting type, which is obtained through fitting numerous data of micro-tube experiments. The exponent of pressure gradient is non-integer and the dimensions at the two ends of the equation are not equal. This is because the boundary-layer theory is still in the process of exploration and is not mature. When the fluid type is changed, the parameters may need to be modified to fit the curve. We show a method to calculate the thickness of the boundary layer rather than a universally accepted expression.

2.3 PTR Distributions for Tight Reservoirs

To determine the relationship between the pores and the permeability, the PTR distribution should be characterized first. For tight reservoirs, pore throats size has a relatively wide distribution, which may range from nanoscale to microscale. Therefore, we could not use one uniform PTR to describe constitution of the pore throats. Figure 5 shows the distribution of PTR in tight oil reservoirs.

Based on statistical analysis of pore size, it is reasonable to use Gaussian function to represent the pore distribution, and the proportion of micro-tubes of radius r_i can be expressed as:

$$f(r_i) = \frac{1}{\sqrt{2\pi}\sigma} \exp\left(-\frac{(r_i - \nu)^2}{2\sigma^2}\right) \tag{2}$$

We could possibly use other functions to represent the pore distribution; the principle to select a function includes two aspects: accuracy in characterization of pore distribution and the convenience for calculation (discussed later) (Table 2).

Because of the boundary layer, the effective pore radius for fluid flow is smaller than the actual pore radius. The effective pore radius can be obtained by deducting the thickness of the boundary layer from the actual pore radius. Therefore, the distribution of the effective pore radius will vary from that of the total pore radius. For conventional and some low-permeability

Table 2 Characteristic values of different pore throat distributions

Pattern	Maximum throat radius (μm)	Mean pore radius (μm)
a	22	10
b	11	5
c	1.1	0.5

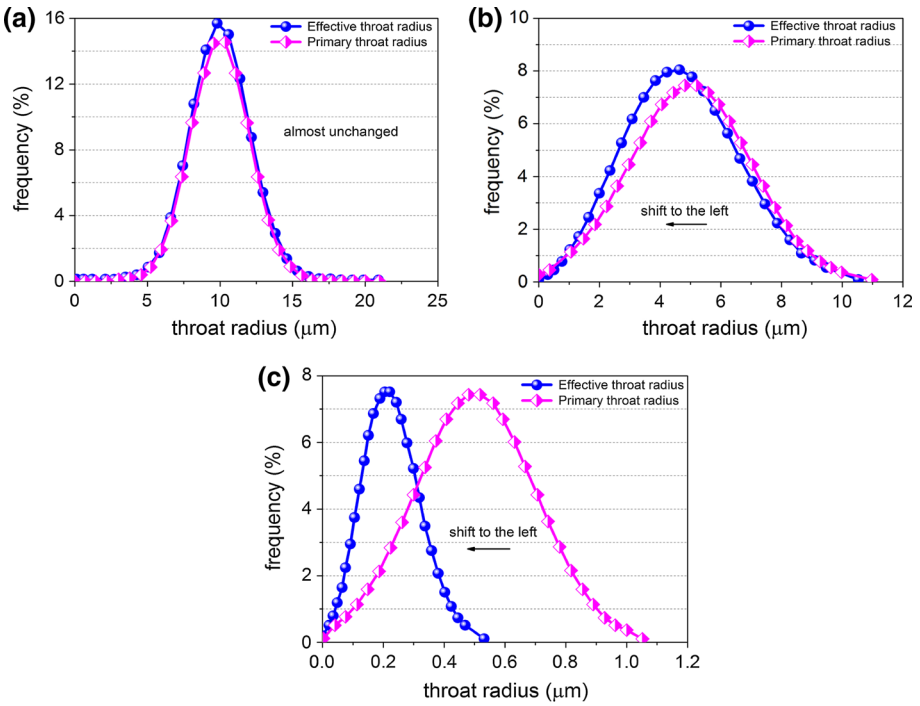

Fig. 6 Comparison of effective and primary pore throat radius with different throat distribution **a** conventional reservoirs, **b** low-permeability reservoirs, **c** tight reservoirs

reservoirs such as shown in Fig. 6a and b, the differences between the two curves are small. This is because the proportion of the boundary layer can be neglected when the pore radius is relatively large. For tight reservoirs, such as shown in Fig. 6c, the distinctions between the two curves are obvious, which is because the boundary layer occupies a large proportion of the pore radius. Therefore, the effective pore radius curve is quite different from the total pore radius curve for tight reservoirs.

2.4 Permeability Model

For fluid flow in the micro-tubes of radius r_i, the flow rate can be described by Poiseuille Equation:

$$Q_i = N\frac{\pi r_i^4 \Delta P}{8\mu\tau L} \tag{3}$$

For tight reservoirs, we should consider the pore distribution, so that Eqs. 2 and 3 are coupled to achieve the flow rate of a bunch of micro-tubes in serial radii given by the Gaussian function (Eq. 4):

$$Q = \frac{\sum_{i=1}^{i=n} \pi N f(r_i) r_i^4 \cdot \Delta P}{8\mu\tau L} \tag{4}$$

For fluid flowing in porous media, the flow rate can also be described by Darcy Law:

$$Q = \frac{K_m A \Delta P}{\mu L} \tag{5}$$

where, A is the cross-sectional area of the rock. For a section with a bunch of tubes in serial radii, the area could be calculated by

$$A = \frac{\sum_{i=1}^{i=n} \pi N f(r_i) r_i^2}{\varphi_m} \tag{6}$$

Substituting Eq. 6 into Eq. 5, we obtain the flow rate:

$$Q = \frac{K_m \sum_{i=1}^{i=n} \pi N f(r_i) r_i^2 \cdot \Delta P}{\varphi_m \mu L} \tag{7}$$

By combining Eqs. 4 and 7, the permeability of the reservoir is expressed as follows:

$$K_m = \frac{\varphi_m \sum_{i=1}^{i=n} \left[\exp\left(-\frac{(r_i - \nu)}{2\sigma^2} \right)^2 r_i^4 \right]}{8\tau \sum_{i=1}^{i=n} \left[\exp\left(-\frac{(r_i - \nu)}{2\sigma^2} \right)^2 r_i^2 \right]} \tag{8}$$

It should be noted that the boundary-layer effect is not considered in Eq. 8, but for the tight oil reservoirs, the boundary-layer effect is very important because of the tiny pore throats. The thickness of the boundary layer should be deducted from the actual radius, so that we could use Eq. 1 to achieve effective pore radius, and then correct Eq. 8 to calculate permeability. By considering boundary-layer effect, the effective permeability is expressed as

$$K_m = \begin{cases} \dfrac{\varphi_m \sum_{i=1}^{i=n} \left[\exp\left(-\frac{(r_i - \nu)}{2\sigma^2} \right)^2 (r_i - r_i \cdot 0.25763 e^{-0.261 r_i} (\nabla P)^{-0.419} \cdot \mu)^4 \right]}{8\tau \sum_{i=1}^{i=n} \left[\exp\left(-\frac{(r_i - \nu)}{2\sigma^2} \right)^2 (r_i - r_i \cdot 0.25763 e^{-0.261 r_i} (\nabla P)^{-0.419} \cdot \mu)^2 \right]}, & \nabla P < 1\,\text{MPa/m} \\ \dfrac{\varphi_m \sum_{i=1}^{i=n} \left[\exp\left(-\frac{(r_i - \nu)}{2\sigma^2} \right)^2 (r_i - r_i \cdot 0.25763 e^{-0.261 r_i} \cdot \mu)^4 \right]}{8\tau \sum_{i=1}^{i=n} \left[\exp\left(-\frac{(r_i - \nu)}{2\sigma^2} \right)^2 (r_i - r_i \cdot 0.25763 e^{-0.261 r_i} \cdot \mu)^2 \right]}, & \nabla P > 1\,\text{MPa/m} \end{cases} \tag{9}$$

3 Model Validation

We use the experimental results (Wang et al. 2008) to test the accuracy of the new permeability model. In Wang's research, the pore size was measured with mercury porosimetry and permeability was measured by displacement experiments with core samples from Yanchang Formation in Ordos Basin (Tables 3, 4). Because the mercury porosimetry and oil permeability cannot be tested in the same core sample, the porosity and air permeability were tested first, and then we achieve the oil permeability by the correlation between oil permeability

Table 3 Reservoir parameters of Yanchang formation

Parameters	No. 1	No. 2	No. 3	No. 4	No. 5	No. 6	No. 7	No. 8
Porosity (%)	8.20	6.20	12.70	8.40	6.80	6.00	5.10	12.10
Air Perm ($10^{-3} \times \mu m^2$)	0.40	0.16	0.12	0.18	0.10	0.10	0.05	0.23
Oil Perm ($10^{-3} \times \mu m^2$)	0.014	0.006	0.004	0.005	0.003	0.003	0.001	0.01

Table 4 Data of pore distributions of Yanchang Formation

Pore size (μm)	No. 1 (%)	No. 2 (%)	No. 3 (%)	No. 4 (%)	No. 5 (%)	No. 6 (%)	No. 7 (%)	No. 8 (%)
0–0.01	38.41	27.42	5.52	52.03	46.86	38.69	66.50	7.31
0.01–0.02	9.12	20.21	12.61	9.70	8.34	15.58	9.04	16.23
0.02–0.05	15.84	17.42	29.65	17.41	11.35	21.59	8.78	17.56
0.05–0.10	12.62	10.43	19.56	10.94	11.21	13.09	5.98	10.25
0.10–0.20	12.17	9.31	15.5	2.95	11.05	4.07	3.09	12.34
0.20–0.30	6.73	8.12	9.51	1.66	5.54	2.11	1.77	11.21
0.30–0.40	2.78	3.84	4.76	0.91	1.64	0.91	0.86	8.65
0.40–0.50	1.11	2.22	1.52	0.57	0.36	0.48	0.42	8.64
0.50–0.60	0.51	1.01	0.78	0.32	0.21	0.25	0.28	4.76
0.60–1.00	0.31	0.37	0.65	0.26	0.14	0.13	0.22	3.05

Tables 3 and 4 are from the experiment data of Wang et al. (2008)

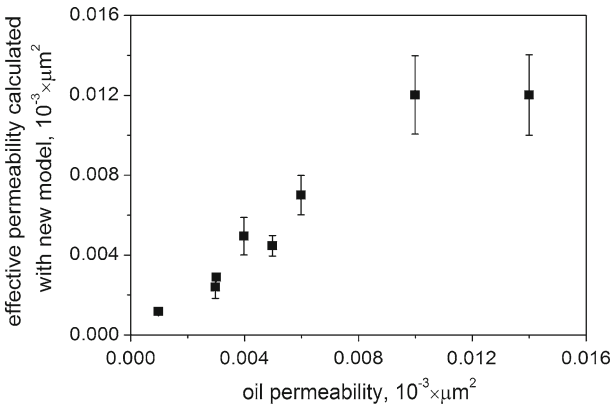

Fig. 7 Comparison between experimental data and calculated data from the model

and gas permeability shown in Fig. 3 and the correlation was measured with core samples in the same formation.

Based on the pore distributions and other related reservoir parameters, the effective permeability of the core samples can be calculated with the new model (Eq. 9). The comparison between experimental data and the calculated data from the model are shown in Fig. 7. The error line gives the differences between experimental data and calculated data. The results show that the calculated permeability has a good match to the permeability from experiment.

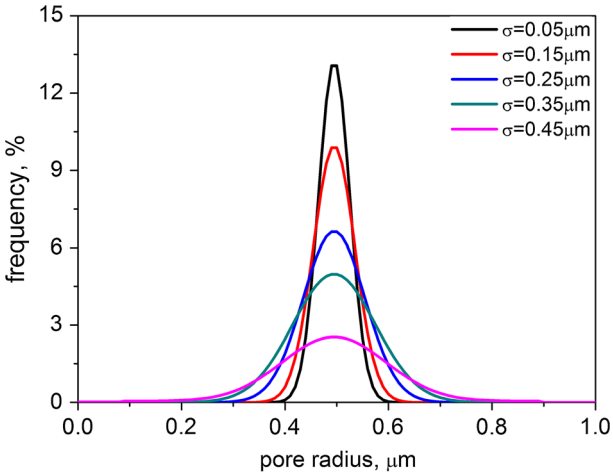

Fig. 8 Pore distributions with various standard deviations and a constant mean pore radius at 0.5 μm

The accurate match suggests a high reliability of the model for calculating the effective permeability of tight oil reservoirs.

4 Influential Variables and Sensitivity Analysis

4.1 Influential Variables

When the pore distribution is represented by Gaussian distribution, two parameters determine the pore throats distribution, the mean and the standard deviation of pore radius. Variations in these two parameters will change pore constitution and also the permeability. Moreover, displacement pressure gradients will also affect the thickness of boundary layer and thus affect the effective permeability.

4.1.1 Effects of Standard Deviation of Pore Radius

In tight reservoirs, pore throats distribute in a quite wide range. Since we use a Gaussian distribution, the mean and standard deviation are used to describe the range of the pores. For example, assuming a mean of 0.5 μm ($\upsilon = 0.5\,\mu$m) for the pore radius, the Gaussian distributions for various standard deviations ($\sigma = 0.05$, 0.15, 0.25, 0.35 and 0.45 μm) of the pore radius are shown in Fig. 8.

By combining a varying mean and a varying standard deviation in pore radii (Fig. 8), we calculate the effective permeability using the model presented earlier (Eq. 9). The permeability from the model (Fig. 9) shows that the effective permeability increases as a function of increasing standard deviation. However, the rate of increase is getting smaller as the mean pore radius increases. This is because when the standard deviation increases, the range of the pore distribution will become wider. This implies a greater proportion of larger pore, and the contribution of these larger pores to permeability will increase. Moreover, it should be noted that the mean pore radius also has a significant impact on permeability, especially when the standard deviation is small.

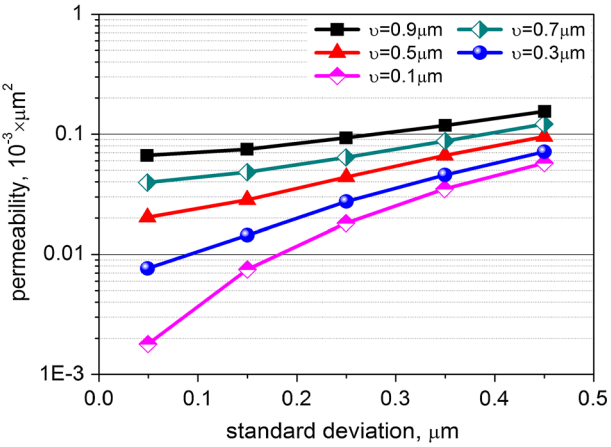

Fig. 9 Relationship between the standard deviation and permeability for several mean pore radii. Standard deviation σ changes from 0.05 to 0.45 μm and mean pore radius υ changes from 0.1 to 0.9 μm

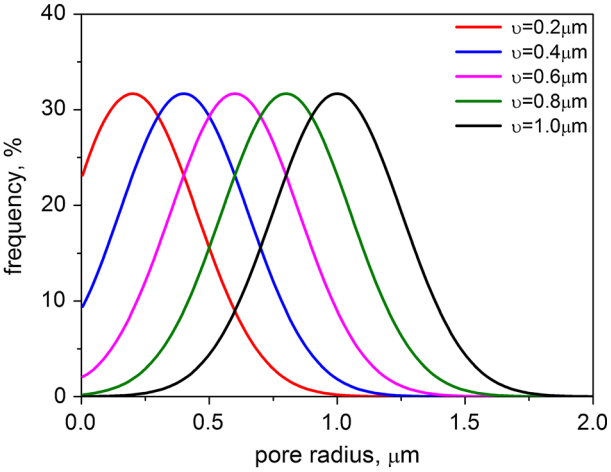

Fig. 10 PTR distributions with different mean pore radii and a constant standard deviation

4.1.2 Effects of the Mean Pore Radius

The mean pore radius is one of the most important factors to characterize a pore distribution, and it plays a fundamental role for determining the permeability of tight oil reservoirs. We constructed several pore distributions with different mean pore radius and constant standard deviation (Fig. 10) and then calculated the effective permeability using our model (Eq. 9).

The permeability is calculated with different mean pore radii and a constant standard deviation (Fig. 11). As seen, the permeability increases with the mean pore radius for a given standard deviation. The smaller the standard deviation is, the faster the increasing rate of permeability will be. This is simply because when the mean pore radius increases, the overall pores will become larger so that the permeability will increase.

Furthermore, the experiments have shown that the effective permeability is more affected by the standard deviation for smaller mean pore radius ($\upsilon < 0.5$ μm in Figs. 9, 11) than for

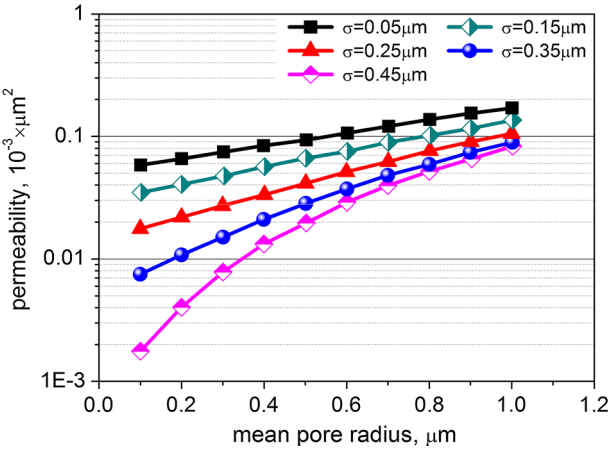

Fig. 11 Relationship between mean pore radius and permeability for several standard deviations

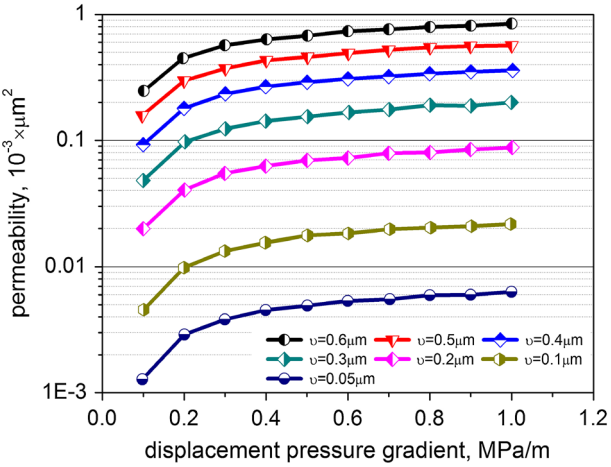

Fig. 12 Relationship between displacement pressure gradient and permeability for several mean pore radii from 0.05 to 0.6 μm and constant standard deviation 0.15 μm

larger mean pore radius. Therefore, it is important to take consideration of pore distributions in describing and calculating the permeability for tight oil reservoirs.

4.1.3 Effects of Displacement Pressure Gradient

High displacement pressure gradients could increase the flow rate and shear force on surface of rock, and this force will affect the thickness of boundary layer and thus the effective permeability. The effect of displacement pressure gradient is considered in the new model (Eqs. 1 and 9). Figure 12 shows the calculated permeability from the new model (Eq. 9) with different displacement pressure gradient under different mean pore radii ranging from 0.05 to 0.6 μm and a constant standard deviation of 0.15 μm.

As seen (Fig. 12), the permeability will increase with the increase in pressure gradient; however, the permeability becomes stable under high pressure gradient. This is because the

thickness of the boundary layer will decrease with the increasing displacement pressure gradient, and the effective pores radius will increase. Moreover, the boundary layer almost changes to the solid boundary layer under high displacement pressure gradient and the effective permeability will become nearly constant eventually.

4.2 Effects of Fluids

For the porous media with low permeability due to small pores, the air permeability is different from liquid permeability (oil permeability or water permeability). The main reason is that gas flow is not significantly affected by the boundary layer, but more affected by gas slippage (Kleinberg effect, Fig. 2c), and thus, the Poiseuille Equation of gas flow is

$$q = \frac{\pi r^4}{16\mu L}\left(1 + \frac{4}{r}\frac{\mu}{\varepsilon}\right)\frac{\Delta P^2}{P_0} \tag{10}$$

where, p_0 is the barometric pressure, μ/ε is the slip coefficient.

For gas flow, the air permeability can be obtained from Eq. 10 by considering the Kleinberg effect, such as

$$K_{airm} = \frac{\varphi_m \sum_{i=1}^{i=n}\left[\exp\left(-\frac{(r_i-\nu)}{2\sigma^2}\right)^2 r_i^4\left(1+\frac{4}{r_i}\frac{\mu}{\varepsilon}\right)\right]}{8\tau\sum_{i=1}^{i=n}\left[\exp\left(-\frac{(r_i-\nu)}{2\sigma^2}\right)^2 r_i^2\right]} \tag{11}$$

In order to represent the differences between them, we define the parameter α as the quotient between air permeability and liquid permeability as expressed in the following equation:

$$\alpha = \begin{cases} \dfrac{\dfrac{\sum_{i=1}^{i=n}\left[\exp\left(-\frac{(r_i-\nu)}{2\sigma^2}\right)^2 r_i^4\left(1+\frac{4}{r_i}\frac{\mu}{\varepsilon}\right)\right]}{\varphi_m\sum_{i=1}^{i=n}\left[\exp(-\frac{(r_i-\nu)}{2\sigma^2})^2 r_i^2\right]}}{\dfrac{\sum_{i=1}^{i=n}\left[\exp\left(-\frac{(r_i-\nu)}{2\sigma^2}\right)^2 (r_i - r_i\cdot 0.25763e^{-0.261 r_i(\nabla P)-0.419\cdot\mu})^4\right]}{\sum_{i=1}^{i=n}\left[\exp\left(-\frac{(r_i-\nu)}{2\sigma^2}\right)^2 \left(r_i - r_i\cdot 0.25763e^{-0.261 r_i(\nabla P)-0.419\cdot\mu}\right)^2\right]}}, & \nabla P < 1\,\text{MPa/m} \\ \dfrac{\dfrac{\sum_{i=1}^{i=n}\left[\exp\left(-\frac{(r_i-\nu)}{2\sigma^2}\right)^2 r_i^4\left(1+\frac{4}{r_i}\frac{\mu}{\varepsilon}\right)\right]}{\varphi_m\sum_{i=1}^{i=n}\left[\exp\left(-\frac{(r_i-\nu)}{2\sigma^2}\right)^2 r_i^2\right]}}{\dfrac{\sum_{i=1}^{i=n}\left[\exp\left(-\frac{(r_i-\nu)}{2\sigma^2}\right)^2 \left(r_i - r_i\cdot 0.25763e^{-0.261 r_i\cdot\mu}\right)^4\right]}{\sum_{i=1}^{i=n}\left[\exp\left(-\frac{(r_i-\nu)}{2\sigma^2}\right)^2 \left(r_i - r_i\cdot 0.25763e^{-0.261 r_i\cdot\mu}\right)^2\right]}}, & \nabla P > 1\,\text{MPa/m} \end{cases} \tag{12}$$

We have investigated the changes of parameter α as a function of the displacement pressure gradient and the pore distribution, and the results are shown in Fig. 13.

As seen (Fig. 13), with the increase in displacement pressure gradient, the parameter α will decrease rapidly and eventually become almost constant. When the displacement pressure gradient is low, liquid flow only happens in the larger pore throats, while gas can flow through all pore throats, and the value of α is large. With the increase in displacement pressure gradient, liquid flow can also happen in narrower pore throats. As there will be more pore throats contributing to the permeability, the permeability to liquid will increase and the value of α will decrease. However, α is still greater than 1 even when the displacement pressure gradient reaches 1.0 MPa/m. This is because the solid boundary layer always exists

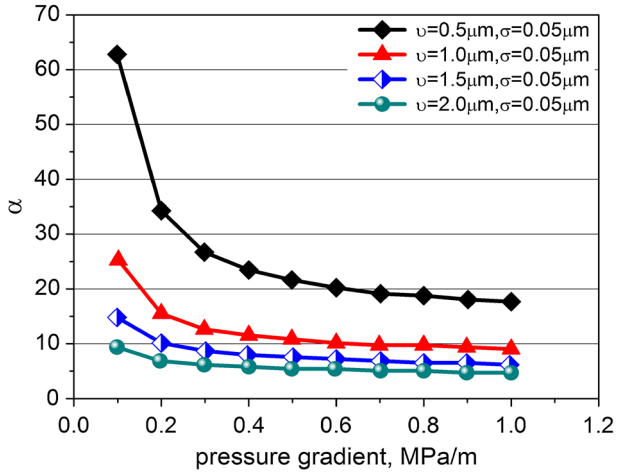

Fig. 13 Relationship between displacement pressure gradient and parameter α

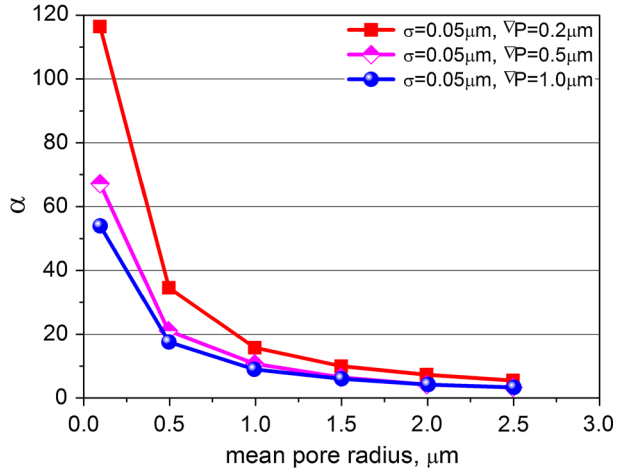

Fig. 14 Relationship between mean pore radius and parameter α under different displacement pressure gradients. Mean pore radius υ changes from 0.1 to 2.5 μm and displacement pressure gradient ∇P changes from 0.2 to 1.0 MPa/m

and restricts the flow. The effective flow radius to liquid will always be narrower than that to gas.

Figure 14 shows that with the increase in the mean pore radius, the parameter α will decrease drastically and become almost constant when the pores are large enough. The tendency for α is similar under different displacement pressure gradients. When the mean pore radius is small, liquid flow is extremely difficult in comparison with the gas flow, and the value of α is large. The liquid flow will become much easier when the mean pore radius increases so that the oil permeability will become similar to air permeability and α is small.

5 Conclusions

Permeability is one of the most critical parameters for reservoir development, especially for tight oil reservoirs. In this study, a new method for calculation of permeability considering the pore distribution and boundary layer has been proposed. A mercury-based experiment providing the heterogeneity of the pore distribution is well utilized in our work. The pore distribution is incorporated in the expression of permeability to account for the effect of heterogeneity in this work. The conclusions can be made as follows:

1. For tight oil reservoirs, the boundary-layer effect plays an important role for determining the reservoir permeability, especially when the pore size is similar to the thickness of boundary layer. The boundary layer will drastically reduce the effective flow radius of pore throats.
2. The mean and standard deviation of pore radius are two basic parameters that describe the distributions of the pore throats. The permeability will change as a function of these two parameters.
3. The air permeability is mainly affected by gas slippage, and it is confirmed by experimental data. The ratio of air permeability and liquid permeability for tight reservoirs was obtained with different pore parameters in the study.

Acknowledgments We acknowledge that this study was partially funded by the Beijing Natural Science foundation (No. 3144033), the Specialized Research Fund for the Doctoral Program of Higher Education (No. 20130007120014), the National Natural Science Foundation of China (E040351304220) and China University of Petroleum, Beijing (No.2462015YQ0206).

References

Banavar, J.R., Johnson, D.L.: Characteristic pore sizes and transport in porous media. Phys. Rev. B **35**(13), 7283 (1987)

Bernabé, Y., Bruderer, C.: Effect of the variance of pore size distribution on the transport properties of heterogeneous networks. J. Geophys. Res. **103**(B1), 513–525 (1998)

Brooks, R.H., Corey, A.T.: Properties of porous media affecting fluid flow. J. Irrig. Drain. Div. **92**(2), 61–90 (1966)

Burdine, N.: Relative permeability calculations from pore size distribution data. J. Petrol. Technol. **5**(3), 71–78 (1953)

Camp, W.K.: Pore-throat sizes in sandstones, tight sandstones, and shales: discussion. AAPG Bull. **95**(8), 1443–1447 (2011)

Carman, P.C.: Fluid flow through granular beds. Trans. Inst. Chem. Eng. **15**, 150–166 (1937)

Carman, P.C.: Flow of Gases Through Porous Media. Academic Press, London (1956)

Carman, P.C.: Fluid flow through granular beds. Chem. Eng. Res. Des. **75**, S32–S48 (1997)

Corey, A.T.: The interrelation between gas and oil relative permeabilities. Prod. Mon. **19**(1), 38–41 (1954)

Dabbous, M.K., Reznik, A.A., Taber, J.J., et al.: The permeability of coal to gas and water. Soc. Petrol. Eng. **14**(06), 563–572 (1974)

Daixun, C.: Gas slippage phenomenon and change of permeability when gas flows in tight porous media. Acta Mech. Sin. Chin. Ed. **34**(1), 96–100 (2002)

Desbois, G., Urai, J.L., Kukla, P.A., et al.: High-resolution 3D fabric and porosity model in a tight gas sandstone reservoir: a new approach to investigate microstructures from mm-to nm-scale combining argon beam cross-sectioning and SEM imaging. J. Petrol. Sci. Eng. **78**(2), 243–257 (2011)

Klinkenberg, L.J.: The permeability of porous media to liquids and gases. In Drilling and Production Practice. American Petroleum Institute (1941)

Kozeny, J.: Über kapillare Leitung des Wassers im Boden: (Aufstieg, Versickerung und Anwendung auf die Bewässerung). Hölder-Pichler-Tempsky (1927)

Latour, L.L., Kleinberg, R.L., Mitra, P.P., et al.: Pore-size distributions and tortuosity in heterogeneous porous media. J. Magn. Reson. A **112**(1), 83–91 (1995)

Li, K., Horne, R.N.: Gas slippage in two-phase flow and the effect of temperature. In SPE Western Regional Meeting. Society of Petroleum Engineers (2001)
Li, K., Horne, R.N.: Experimental study of gas slippage in two-phase flow. SPE 89038. Reserv. Eval. Eng. **7**(06), 409–415 (2004)
Li, Z., He, S.: Influence of boundary layers upon filtration law in low-permeability oil reservoirs. Petrol. Geol. Oilfield Dev. Daqing **2**, 57–59 (2005)
Li, Y., Lei, Q., Liu, X.G., et al.: Characteristics of micro scale nonlinear filtration. Petrol. Explor. Dev. **38**(3), 336–340 (2011)
Li, W.C., Zhang, Y.M., Wang, F.: Application of constant-rate mercury penetration technique to study of pore throat characteristics of tight reservoir: A case study from the Upper Triassic Yanchang Formation in Ordos Basin. Lithol. Reserv. **24**(6), 60–65 (2012)
Mala, G.M., Li, D.: Flow characteristics of water in microtubes. Int. J. Heat Fluid Flow **20**(2), 142–148 (1999)
Мархасин И Л. Физико-химическая механика нефтяното пласта. М: Недра, 1977:14
Nelson, P.H.: Pore-throat sizes in sandstones, tight sandstones, and shales. AAPG Bull. **93**(3), 329–340 (2009)
Purcell, W.R.: Capillary pressures-their measurement using mercury and the calculation of permeability therefrom. J. Petrol. Technol. **1**(2), 39–48 (1949)
Riepe, L., Suhaimi, M.H., Kumar, M., et al.: Application of high resolution micro-CT imaging and pore network modeling (PNM) for the petrophysical characterization of tight gas reservoirs—a case history from a deep clastic tight gas reservoir in Oman. Soc. Petrol. Eng. **142472**, 31 (2011)
Sampath, K., Keighin, C.W.: Factors affecting gas slippage in tight sandstones of cretaceous age in the Uinta basin. J. Petrol. Technol. **34**(11), 2715–2720 (1982)
Tian, X., Cheng, L., Yan, Y., et al.: An improved solution to estimate relative permeability in tight oil reservoirs. J. Petrol. Explor. Prod. Technol. **5**(3), 1–10 (2014)
Wang, R.F., Cheng, M.Q., Sun, W.: The research of micro-pore structure in super-low permeability sandstone reservoir of the Yanchang formation in Ordos Basin. Geol. Rev. **54**(2), 270–277 (2008)
Wang, R.F., Shen, P.P., Song, Z.Q., et al.: Characteristics of micro-pore throat in ultra-low permeability sandstone reservoir. Acta Petroiei Sin. **30**(4), 560–563 (2009)
Xu, S., Yue, X.: Experimental research on nonlinear flow characteristics at low velocity. J. China Univ. Petrol. (Nat. Sci. Ed.) **5**, 014 (2007)
Yang, Z.M., Liu X.G., Zhang Z.H., et al.: Evaluation of reservoir classification and numerical simulation of well pattern optimization in ultra-low permeability reservoirs, pp. 50–51. Petroleum Industry Press, Beijing (2012) (**In Chinese**)
Youssef, S., Rosenberg, E., Gland, N.F., et al.: High resolution CT and pore-network models to assess petrophysical properties of homogeneous and heterogeneous carbonates. In EAGE Reservoir Characterization and Simulation Conference. Society of Petroleum Engineers. (2007)
Zhang, P., Zhang, L., Li, W., et al.: Experiment on the influence of boundary layer on the Non-Darcy seepage law. J. Hebei Univ. Eng. (Nat. Sci. Ed.) **3**, 019 (2008)